Editors' Suggestion | Featured in Physics

Properties of Cosmic Lithium Isotopes Measured by the Alpha Magnetic Spectrometer

M. Aguilar,[29] G. Ambrosi,[35] H. Anderson,[10] L. Arruda,[27] N. Attig,[24] C. Bagwell,[10] F. Barao,[27] M. Barbanera,[35] L. Barrin,[14] A. Bartoloni,[39] R. Battiston,[46,47] A. Bayyari,[20] N. Belyaev,[10] B. Bertucci,[35,36] V. Bindi,[20] K. Bollweg,[21] J. Bolster,[10] M. Borchiellini,[17] B. Borgia,[39,40] M. J. Boschini,[31] M. Bourquin,[15] C. Brugnoni,[35,36] J. Burger,[10] W. J. Burger,[46] N. Burzillà,[41] X. D. Cai,[10] M. Capell,[10] J. Casaus,[29] G. Castellini,[13] F. Cervelli,[37] Y. H. Chang,[44] G. M. Chen,[6,7] G. R. Chen,[23] H. Chen,[19] H. S. Chen,[6,7] Y. Chen,[23] L. Cheng,[23] H. Y. Chou,[44] S. Chouridou,[1] V. Choutko,[10] C. H. Chung,[1] C. Clark,[10,21] G. Coignet,[3] C. Consolandi,[20] A. Contin,[8,9] C. Corti,[20] Z. Cui,[22,23] K. Dadzie,[10] F. D'Angelo,[9,8] A. Dass,[46,47] C. Delgado,[29] S. Della Torre,[31] M. B. Demirköz,[2] L. Derome,[16] S. Di Falco,[37] V. Di Felice,[41] C. Díaz,[29] F. Dimiccoli,[46,47] P. von Doetinchem,[20] F. Dong,[33] M. Duranti,[35] A. Egorov,[10] A. Eline,[10] F. Faldi,[35,36] D. Fehr,[1] J. Feng,[18] E. Fiandrini,[35,36] P. Fisher,[10] V. Formato,[41] R. J. García-López,[26] C. Gargiulo,[14] H. Gast,[1] M. Gervasi,[31,32] F. Giovacchini,[29] D. M. Gómez-Coral,[30] J. Gong,[33] D. Grandi,[31,32] M. Graziani,[35,36] S. Haino,[44] K. C. Han,[28] Z. H. He,[18] B. Heber,[25] F. Hernández-Nicolás,[29] T. H. Hsieh,[10] J. Y. Hu,[35] B. W. Huang,[19] M. Ionica,[35] M. Incagli,[37] Yi Jia,[10] H. Jinchi,[28] G. Karagöz,[2] Th. Kirn,[1] A. P. Klipfel,[10] O. Kounina,[10] A. Kounine,[10] V. Koutsenko,[10] D. Krasnopevtsev,[10] A. Kuhlman,[20] A. Kulemzin,[10] G. La Vacca,[31,32] E. Laudi,[14] G. Laurenti,[8] G. LaVecchia,[10] I. Lazzizzera,[46,47] H. T. Lee,[43] S. C. Lee,[44] H. L. Li,[23] J. H. Li,[22] J. Q. Li,[33] M. Li,[15] M. Li,[22] Q. Li,[33] Q. Li,[22] Q. Y. Li,[23] S. L. Li,[6] Z. H. Li,[6,7] M. J. Liang,[6,7] P. Liao,[22] C. H. Lin,[44] T. Lippert,[24] J. H. Liu,[5] P. C. Liu,[23] Z. Liu,[41] S. Q. Lu,[6,44] J. Z. Luo,[33] Q. Luo,[18] S. D. Luo,[19] Xi Luo,[23] C. Mañá,[29] J. Marín,[29] J. Marquardt,[25] G. Martínez,[29] N. Masi,[8] D. Maurin,[16] T. Medvedeva,[10] A. Menchaca-Rocha,[30] Q. Meng,[33] V. V. Mikhailov,[23] M. Molero,[26] P. Mott,[10,21] L. Mussolin,[35,36] Y. Najafi Jozani,[1] R. Nicolaidis,[47,46] N. Nikonov,[20] F. Nozzoli,[46] J. Ocampo-Peleteiro,[29] A. Oliva,[8] M. Orcinha,[35,36] F. Palmonari,[8,9] M. Paniccia,[15] A. Pashnin,[10] M. Pauluzzi,[35,36] D. Pelosi,[35,36] S. Pensotti,[31,32] P. Pietzcker,[25] V. Plyaskin,[10] S. Poluianov,[34] D. Pridöhl,[1] Z. Y. Qu,[23] L. Quadrani,[8,9] P. G. Rancoita,[31] D. Rapin,[15] A. Reina Conde,[8] E. Robyn,[8] I. Rodríguez-García,[29] L. Romaneehsen,[25] F. Rossi,[47,46] A. Rozhkov,[10] D. Rozza,[31,32] R. Sagdeev,[11] S. Schael,[1] A. Schultz von Dratzig,[1] G. Schwering,[1] E. S. Seo,[12] B. S. Shan,[4] A. Shukla,[20] T. Siedenburg,[1] A. Siemko,[10] G. Silvestre,[35] J. W. Song,[22] X. J. Song,[23] R. Sonnabend,[1] L. Strigari,[39,*] T. Su,[23] Q. Sun,[22] Z. T. Sun,[6] L. Tabarroni,[41] M. Tacconi,[31,32] Z. C. Tang,[6] J. Tian,[41] Y. Tian,[19] Samuel C. C. Ting,[10,14] S. M. Ting,[10] N. Tomassetti,[35,36] J. Torsti,[48] B. Türk,[2] A. Ubaldi,[35,36] T. Urban,[10,21] I. Usoskin,[34] V. Vagelli,[38,35] R. Vainio,[48] P. Väisänen,[35,36] M. Valencia-Otero,[45] E. Valente,[39,40] E. Valtonen,[48] M. Vázquez Acosta,[26] M. Vecchi,[17] M. Velasco,[29] C. X. Wang,[22] J. C. Wang,[6] L. Wang,[5] L. Q. Wang,[22] N. H. Wang,[22] Q. L. Wang,[5] S. Wang,[20] X. Wang,[10] Z. M. Wang,[23] J. Wei,[15,23] Z. L. Weng,[10] H. Wu,[33] Y. Wu,[23] Z. B. Wu,[22] J. N. Xiao,[19] R. Q. Xiong,[33] X. Z. Xiong,[19] W. Xu,[22,23] Q. Yan,[6,7] H. T. Yang,[6,7] Y. Yang,[42] H. Yi,[33] Y. H. You,[6,7] Y. M. Yu,[10] Z. Q. Yu,[6] C. Zhang,[6] F. Z. Zhang,[6] J. Zhang,[22] J. H. Zhang,[33] Z. Zhang,[10] P. W. Zhao,[18] C. Zheng,[23] Z. M. Zheng,[4] H. L. Zhuang,[6] V. Zhukov,[1] A. Zichichi,[8,9] M. Zuberi,[10] and P. Zuccon[46,47]

(AMS Collaboration)

[1]*I. Physics Institute and JARA-FAME, RWTH Aachen University, 52056 Aachen, Germany*
[2]*Department of Physics, Middle East Technical University (METU), 06800 Ankara, Türkiye*
[3]*Université Grenoble Alpes, Université Savoie Mont Blanc, CNRS, LAPP-IN2P3, 74000 Annecy, France*
[4]*Beihang University (BUAA), Beijing, 100191, China*
[5]*Institute of Electrical Engineering (IEE), Chinese Academy of Sciences, Beijing, 100190, China*
[6]*Institute of High Energy Physics (IHEP), Chinese Academy of Sciences, Beijing, 100049, China*
[7]*University of Chinese Academy of Sciences (UCAS), Beijing, 100049, China*
[8]*INFN Sezione di Bologna, 40126 Bologna, Italy*
[9]*Università di Bologna, 40126 Bologna, Italy*
[10]*Massachusetts Institute of Technology (MIT), Cambridge, Massachusetts 02139, USA*
[11]*East-West Center for Space Science, University of Maryland, College Park, Maryland 20742, USA*
[12]*IPST, University of Maryland, College Park, Maryland 20742, USA*
[13]*CNR–IROE, 50125 Firenze, Italy*
[14]*European Organization for Nuclear Research (CERN), 1211 Geneva 23, Switzerland*
[15]*DPNC, Université de Genève, 1211 Genève 4, Switzerland*
[16]*Université Grenoble Alpes, CNRS, Grenoble INP, LPSC-IN2P3, 38000 Grenoble, France*
[17]*Kapteyn Astronomical Institute, University of Groningen, P.O. Box 800, 9700 AV Groningen, Netherlands*

[18]Sun Yat–Sen University (SYSU), Guangzhou, 510275, China
[19]Zhejiang University (ZJU), Hangzhou, 310058, China
[20]Physics and Astronomy Department, University of Hawaii, Honolulu, Hawaii 96822, USA
[21]National Aeronautics and Space Administration Johnson Space Center (JSC), Houston, Texas 77058, USA
[22]Shandong University (SDU), Jinan, Shandong, 250100, China
[23]Shandong Institute of Advanced Technology (SDIAT), Jinan, Shandong, 250100, China
[24]Jülich Supercomputing Centre and JARA-FAME, Research Centre Jülich, 52425 Jülich, Germany
[25]Institut für Experimentelle und Angewandte Physik, Christian-Albrechts-Universität zu Kiel, 24118 Kiel, Germany
[26]Instituto de Astrofísica de Canarias (IAC), 38205 La Laguna, and Departamento de Astrofísica, Universidad de La Laguna, 38206 La Laguna, Tenerife, Spain
[27]Laboratório de Instrumentação e Física Experimental de Partículas (LIP), 1649-003 Lisboa, Portugal
[28]National Chung–Shan Institute of Science and Technology (NCSIST), Longtan, Tao Yuan, 32546, Taiwan
[29]Centro de Investigaciones Energéticas, Medioambientales y Tecnológicas (CIEMAT), 28040 Madrid, Spain
[30]Instituto de Física, Universidad Nacional Autónoma de México (UNAM), Ciudad de México, 01000 Mexico
[31]INFN Sezione di Milano–Bicocca, 20126 Milano, Italy
[32]Università di Milano–Bicocca, 20126 Milano, Italy
[33]Southeast University (SEU), Nanjing, 210096, China
[34]Sodankylä Geophysical Observatory and Space Physics and Astronomy Research Unit, University of Oulu, 90014 Oulu, Finland
[35]INFN Sezione di Perugia, 06100 Perugia, Italy
[36]Università di Perugia, 06100 Perugia, Italy
[37]INFN Sezione di Pisa, 56100 Pisa, Italy
[38]Agenzia Spaziale Italiana (ASI), 00133 Roma, Italy
[39]INFN Sezione di Roma 1, 00185 Roma, Italy
[40]Università di Roma La Sapienza, 00185 Roma, Italy
[41]INFN Sezione di Roma Tor Vergata, 00133 Roma, Italy
[42]National Cheng Kung University, Tainan, 70101, Taiwan
[43]Academia Sinica Grid Center (ASGC), Nankang, Taipei, 11529, Taiwan
[44]Institute of Physics, Academia Sinica, Nankang, Taipei, 11529, Taiwan
[45]Physics Department and Center for High Energy and High Field Physics, National Central University (NCU), Tao Yuan, 32054, Taiwan
[46]INFN TIFPA, 38123 Trento, Italy
[47]Università di Trento, 38123 Trento, Italy
[48]Department of Physics and Astronomy, Space Research Laboratory, University of Turku, 20014 Turku, Finland

(Received 19 December 2024; accepted 28 March 2025; published 20 May 2025; corrected 17 July 2025)

We present the first measurement of cosmic-ray fluxes of ^{6}Li and ^{7}Li isotopes in the rigidity range from 1.9 to 25 GV. The measurements are based on 9.7×10^5 ^{6}Li and 1.04×10^6 ^{7}Li nuclei collected by the Alpha Magnetic Spectrometer on the International Space Station from May 2011 to October 2023. We observe that over the entire rigidity range the ^{6}Li and ^{7}Li fluxes exhibit nearly identical time variations and, above ∼4 GV, the time variations of ^{6}Li, ^{7}Li, He, Be, B, C, N, and O fluxes are identical. Above ∼7 GV, we find an identical rigidity dependence of the ^{6}Li and ^{7}Li fluxes. This shows that they are both produced by collisions of heavier cosmic-ray nuclei with the interstellar medium and, in particular, excludes the existence of a sizable primary component in the ^{7}Li flux.

DOI: 10.1103/PhysRevLett.134.201001

Introduction—Lithium nuclei are among the rarest in the Solar System, yet they are relatively common in cosmic rays [1,2]. They consist of two stable isotopes, ^{6}Li and ^{7}Li. Both are thought to be produced by collisions of heavier cosmic-ray nuclei with the interstellar medium; therefore, they are called secondary cosmic rays. In addition, ^{7}Li may also contain a primordial component, produced at the time of the Big Bang, and a primary component, produced from ^{7}Be decay by electron capture at astrophysical sources, such as low-mass stars or novae [3–5]. Lithium is the only

[*]Also at IRCCS Azienda Ospedaliero-Universitaria di Bologna, Bologna, Italy.

element having three or more possible sources in the Cosmos. Establishing the origin of ^{7}Li has an important impact on understanding the formation of the Universe and its chemical evolution. Currently, the origin of ^{7}Li is not well understood. First, the primordial ^{7}Li abundance predicted from Big Bang nucleosynthesis does not match the value inferred from stellar observations and cosmic-ray data [6]. Second, estimates of primordial ^{7}Li abundance from stellar and cosmological observations are in disagreement [7]. Finally, the Alpha Magnetic Spectrometer (AMS) lithium flux (^{6}Li + ^{7}Li) measurement [8,9] could not be described by calculations of the secondary lithium flux by cosmic-ray propagation models. Explicitly, at rigidities above ∼4 GV, an excess over model predictions has been observed and interpreted as either due to the presence of a primary component in the ^{7}Li flux [10] or due to uncertainties on nuclear fragmentation cross sections [11–13]. Precise knowledge of the rigidity dependencies of the cosmic-ray ^{6}Li and ^{7}Li isotope fluxes provides insights into the origin of lithium nuclei.

Over the last 50 years, several experiments have measured the ^{7}Li/^{6}Li ratio as a function of kinetic energy per nucleon below 1.7 GeV/n with ∼20% errors and as a function of rigidity below 6.3 GV with ∼15% uncertainties [14–21]. The lithium isotope fluxes have been measured only below 0.3 GeV/n (below ∼1.9 GV in rigidity) [15].

In this Letter, we present precision measurements of the ^{6}Li and ^{7}Li fluxes in the rigidity range from 1.9 to 25 GV, based on 9.7×10^5 ^{6}Li and 1.04×10^6 ^{7}Li nuclei collected by AMS from May 2011 to October 2023. The total error at 10 GV is 3.3% for both ^{6}Li and ^{7}Li fluxes and 2.2% for ^{7}Li/^{6}Li flux ratio.

Detector—The AMS detector layout and description are presented in Refs. [9,22] and shown in Fig. S1 of Supplemental Material [23]. The elements used in this analysis are the magnet [24], the silicon tracker [25–28], the time of flight counters (TOF) [29], and the ring imaging Čerenkov detector (RICH) [30]. Further information on the AMS layout, performance, trigger, and the Monte Carlo (MC) simulations [31,32] is presented in Supplemental Material [23].

Selection—AMS collected 2.3×10^{11} cosmic-ray events from May 2011 to October 2023. Lithium nuclei events are required to be downward going and to have a reconstructed track in the inner tracker which passes through $L1$, the top layer of the silicon tracker. Charge measurements on $L1$, the upper TOF, the inner tracker, and the lower TOF are required to be compatible with charge number $Z = 3$. Details of the event selection, including the geomagnetic cutoff [33], are provided in Supplemental Material [23] and in Ref. [8]. With this selection, the charge confusion from noninteracting nuclei is negligible (< 0.01%) over the entire rigidity range. The residual background comes from heavier nuclei that interact above tracker $L2$; see discussion and Figs. S2 and S3 in Supplemental Material [23]. This background has been found to be 1.0% for ^{6}Li and 1.1% for ^{7}Li at 2 GV, decreasing with increasing rigidity and becoming 0.1% at 25 GV for both ^{6}Li and ^{7}Li. The additional background for ^{6}Li from the fragmentation of $^7\text{Li} \rightarrow {}^6\text{Li}$ within AMS is estimated from MC simulation and found to be < 1.8% in the entire rigidity range.

Analysis—The fluxes of lithium isotopes $\Phi^{^6\text{Li}}$ and $\Phi^{^7\text{Li}}$ are measured in 28 rigidity bins ranging from 1.9 to 25 GV chosen according to Ref. [8]. The isotropic flux $\Phi_i^{^{\text{A}}\text{Li}}$ in the ith rigidity bin $(R_i, R_i + \Delta R_i)$ is given by

$$\Phi_i^{^{\text{A}}\text{Li}} = \frac{N_i^{\text{A}}}{A_i^{\text{A}} \epsilon_i \Delta R_i T_i}, \tag{1}$$

where A = 6, 7 is the atomic mass number, N_i^{A} is the number of background subtracted events, A_i^{A} is the effective acceptance, ϵ_i is the trigger efficiency, and T_i is the collection time. To compute the N_i^{A}, a procedure based on fitting the inverse mass distribution followed by the unfolding procedure described in Ref. [34] was performed; see a detailed description and Figs. S4 and S5 in Supplemental Material [23]. In total, 9.7×10^5 ^{6}Li and 1.04×10^6 ^{7}Li events were obtained.

Extensive studies were made on the systematic errors. The systematic errors in N_i^{A} are due to uncertainties in the rigidity and velocity resolution functions, fitting and unfolding procedures, and background subtraction. The rigidity resolution function, determined from MC simulation, has been extensively verified with the data [8]. The velocity resolution functions of TOF and RICH [35] were determined from the MC simulation and validated with data; see discussion and Figs. S6–S9 in Supplemental Material [23].

The systematic uncertainty of N_i^{A} due to the uncertainties in the rigidity and velocity resolution functions and due to the fitting and unfolding procedures has been evaluated to be < 2.2% below 4 GV and < 1.8% above 4 GV for both $\Phi^{^6\text{Li}}$ and $\Phi^{^7\text{Li}}$. The systematic uncertainty of N_i^{A} from the background subtraction is < 1.0% for $\Phi^{^6\text{Li}}$ and < 0.5% for $\Phi^{^7\text{Li}}$ over the entire rigidity range.

Other sources of systematic errors include the uncertainties in the trigger efficiency, the geomagnetic cutoff factor, and the acceptance calculation.

The trigger efficiency has been measured as described in Ref. [31]. The systematic error for both fluxes due to the trigger efficiency uncertainties is < 0.3% over the entire rigidity range. The geomagnetic cutoff factor was varied from 1.0 to 1.4, resulting in a negligible systematic uncertainty < 0.1% in the entire rigidity range.

The effective acceptances A_i^{A} were calculated from the MC simulation and then corrected for differences between the data and simulated events related to (a) event reconstruction and selection, namely, in the efficiencies of track finding, charge determination, tracker quality cuts,

and velocity quality cuts, and (b) inelastic interactions of lithium isotopes in the AMS materials. The total correction from (a) and (b) to the effective acceptances was found to be $< 5\%$ over the entire rigidity range. The systematic error on the $\Phi^{^6\mathrm{Li}}$ and $\Phi^{^7\mathrm{Li}}$ associated with (a) has been found to be $< 2\%$ over the entire rigidity range. The material traversed by nuclei within AMS is composed primarily of carbon and aluminum. The survival probability of Li nuclei due to interactions in the materials was measured using cosmic-ray data collected by AMS as described in Ref. [36]. The systematic error associated with (b) on the fluxes was found to be $< 2.2\%$ for $\Phi^{^6\mathrm{Li}}$ and $< 2.3\%$ for $\Phi^{^7\mathrm{Li}}$ over the entire rigidity range.

The variation of the reconstruction and selection efficiencies were studied as a function of time. A time-dependent systematic error due to the variations of reconstruction and selection efficiencies for different time periods was estimated to be $< 1.3\%$ for both fluxes in the entire rigidity range. All the other systematic errors are time independent.

Most importantly, independent analyses were performed on the same data sample by three independent study groups. The results of these analyses are consistent with this Letter.

Results—The $\Phi^{^6\mathrm{Li}}$ and $\Phi^{^7\mathrm{Li}}$ fluxes, and the $\Phi^{^7\mathrm{Li}}/\Phi^{^6\mathrm{Li}}$ flux ratio, have been measured as functions of rigidity from 1.9 to 25 GV in 42 time periods of four Bartels rotations (108 days) each from May 2011 to October 2023 and are tabulated in Tables S1–S42 in Supplemental Material [23,37], including statistical and systematic errors. For the fluxes, the contributions of individual independent sources to the systematic error were added in quadrature to obtain the total systematic uncertainty. For the $\Phi^{^7\mathrm{Li}}/\Phi^{^6\mathrm{Li}}$, the correlation of the systematic errors is taken into account to evaluate the total systematic error. Note, the sum of the measured $\Phi^{^6\mathrm{Li}}$ and $\Phi^{^7\mathrm{Li}}$ is in good agreement with the AMS results of Refs. [8,9] in the overlapping rigidity and time intervals.

The time-averaged $\Phi^{^6\mathrm{Li}}$ and $\Phi^{^7\mathrm{Li}}$, and the $\Phi^{^7\mathrm{Li}}/\Phi^{^6\mathrm{Li}}$, are reported in Table S43 in Supplemental Material [23,37] as functions of rigidity, including statistical and systematic errors.

Figure 1 shows the AMS time-averaged $\Phi^{^7\mathrm{Li}}/\Phi^{^6\mathrm{Li}}$ as a function of kinetic energy per nucleon together with earlier measurements [17–19,21]. Data from other experiments have been extracted using Ref. [38].

Figure 2 shows the AMS $\Phi^{^6\mathrm{Li}}$ and $\Phi^{^7\mathrm{Li}}$ as functions of time for four characteristic rigidity bins, compared with the AMS He flux Φ^{He} [39]. As seen, the $\Phi^{^6\mathrm{Li}}$, $\Phi^{^7\mathrm{Li}}$, and Φ^{He} exhibit nearly identical variations with time and the relative magnitude of the variations decreases with increasing rigidity. This implies that $\Phi^{^6\mathrm{Li}}$ and $\Phi^{^7\mathrm{Li}}$ exhibit variations with time nearly identical to those of Be, B, C, N, and O fluxes [40].

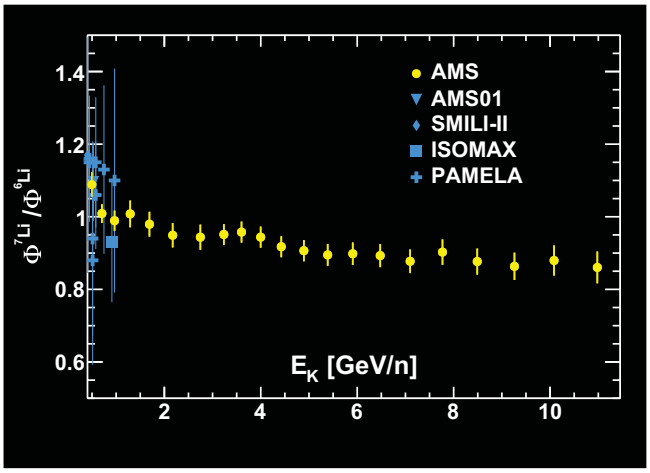

FIG. 1. The AMS $\Phi^{^7\mathrm{Li}}/\Phi^{^6\mathrm{Li}}$ as a function of kinetic energy per nucleon with total errors, together with previous measurements [17–19,21].

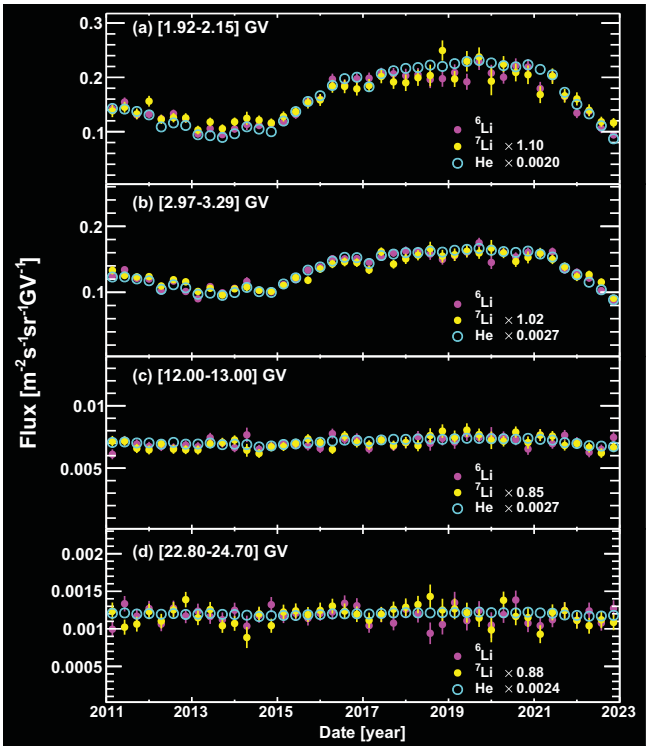

FIG. 2. The AMS $\Phi^{^6\mathrm{Li}}$ (magenta points), $\Phi^{^7\mathrm{Li}}$ (yellow points), and Φ^{He} (cyan open circles) as functions of time for four characteristic rigidity bins (a) [1.92–2.15] GV, (b) [2.97–3.29] GV, (c) [12.00–13.00] GV, and (d) [22.80–24.70] GV. The $\Phi^{^7\mathrm{Li}}$ and Φ^{He} have been scaled to obtain the same time-averaged flux as $\Phi^{^6\mathrm{Li}}$ in each rigidity bin. The errors are the quadratic sum of the statistical and time-dependent systematic errors. As seen, in each rigidity bin the three fluxes show a nearly identical time behavior.

To study the differences in time variation for the $\Phi^{^6\mathrm{Li}}$, $\Phi^{^7\mathrm{Li}}$, and Φ^{He} in detail, we fit a linear relation between the relative variations of $\Phi^{^6\mathrm{Li}}/\Phi^{\mathrm{He}}$ and $\Phi^{^7\mathrm{Li}}/\Phi^{\mathrm{He}}$ and of Φ^{He} for the ith rigidity bin, $(R_i, R_i + \Delta R_i)$, as

$$\frac{\Phi_i^{^6\mathrm{Li}}/\Phi_i^{\mathrm{He}} - \langle \Phi_i^{^6\mathrm{Li}}/\Phi_i^{\mathrm{He}} \rangle}{\langle \Phi_i^{^6\mathrm{Li}}/\Phi_i^{\mathrm{He}} \rangle} = k_i^{^6\mathrm{Li}} \frac{\Phi_i^{\mathrm{He}} - \langle \Phi_i^{\mathrm{He}} \rangle}{\langle \Phi_i^{\mathrm{He}} \rangle}, \quad (2)$$

$$\frac{\Phi_i^{^7\mathrm{Li}}/\Phi_i^{\mathrm{He}} - \langle \Phi_i^{^7\mathrm{Li}}/\Phi_i^{\mathrm{He}} \rangle}{\langle \Phi_i^{^7\mathrm{Li}}/\Phi_i^{\mathrm{He}} \rangle} = k_i^{^7\mathrm{Li}} \frac{\Phi_i^{\mathrm{He}} - \langle \Phi_i^{\mathrm{He}} \rangle}{\langle \Phi_i^{\mathrm{He}} \rangle}, \quad (3)$$

where $k_i^{^6\mathrm{Li}}$ and $k_i^{^7\mathrm{Li}}$ are the slopes of the linear dependence for the ith bin, and $\langle \Phi_i^{^6\mathrm{Li}}/\Phi_i^{\mathrm{He}} \rangle$, $\langle \Phi_i^{^7\mathrm{Li}}/\Phi_i^{\mathrm{He}} \rangle$, and $\langle \Phi_i^{\mathrm{He}} \rangle$ are the averages of $\Phi^{^6\mathrm{Li}}/\Phi^{\mathrm{He}}$, $\Phi^{^7\mathrm{Li}}/\Phi^{\mathrm{He}}$, and Φ^{He} over the entire data taking period, similar to Ref. [41]. Figures S10 and S11 of Supplemental Material [23] show the relative variation of $\Phi^{^6\mathrm{Li}}/\Phi^{\mathrm{He}}$ and $\Phi^{^7\mathrm{Li}}/\Phi^{\mathrm{He}}$ as a function of the relative variation of Φ^{He} for four characteristic rigidity bins, together with the fits with Eqs. (2) and (3), respectively. Figure S12 of Supplemental Material [23] shows the fit results of the slopes $k^{^6\mathrm{Li}}$ and $k^{^7\mathrm{Li}}$ as functions of rigidity from 1.9 to 7.1 GV. As seen, from 1.9 to 3.64 GV, both $k^{^6\mathrm{Li}}$ and $k^{^7\mathrm{Li}}$ are below zero, showing that $\Phi^{^6\mathrm{Li}}$ and $\Phi^{^7\mathrm{Li}}$ are less modulated than Φ^{He} in this rigidity range. From 1.9 to 4.02 GV, $k^{^7\mathrm{Li}}$ is smaller than $k^{^6\mathrm{Li}}$, indicating that $\Phi^{^7\mathrm{Li}}$ is less modulated than $\Phi^{^6\mathrm{Li}}$ in this rigidity range. Above 4.02 GV, $k^{^6\mathrm{Li}}$ and $k^{^7\mathrm{Li}}$ are both compatible with zero, showing that $\Phi^{^6\mathrm{Li}}$, $\Phi^{^7\mathrm{Li}}$, and Φ^{He} exhibit identical variations with time at rigidities higher than ~4 GV. This implies that above ~4 GV, the time variations of $\Phi^{^6\mathrm{Li}}$ and $\Phi^{^7\mathrm{Li}}$ are identical to those of Be, B, C, N, and O fluxes [40].

Figure 3 shows the time-averaged $\Phi^{^6\mathrm{Li}}$ and $\Phi^{^7\mathrm{Li}}$ fluxes as functions of rigidity, together with their time variation. In this and the subsequent figure, the data points are placed along the abscissa at an $\tilde{R}$ calculated for a flux $\propto R^{-2.7}$ [42].

The time-averaged $\Phi^{^7\mathrm{Li}}/\Phi^{^6\mathrm{Li}}$ flux ratio as a function of rigidity is shown in Fig. 4, together with the predictions of the recent propagation models GALPROP [10] and USINE [11] based on AMS lithium flux ($^6\mathrm{Li} + {}^7\mathrm{Li}$) measurement [8,9]. As seen, both models fail to describe the AMS result on $\Phi^{^7\mathrm{Li}}/\Phi^{^6\mathrm{Li}}$. In particular, the USINE model prediction does not agree with the AMS measurements within the model uncertainties that are related to the $^6\mathrm{Li}$ and $^7\mathrm{Li}$ production cross sections from heavier nuclei. Figure S13 of Supplemental Material [23] shows the AMS $\Phi^{^7\mathrm{Li}}/\Phi^{^6\mathrm{Li}}$ together with two predictions of the GALPROP model, which use two different parametrizations [43] of the $^6\mathrm{Li}$ and $^7\mathrm{Li}$ production cross sections but both assume only a secondary origin of the Li isotopes [44]. As seen, neither model prediction agrees with the AMS result.

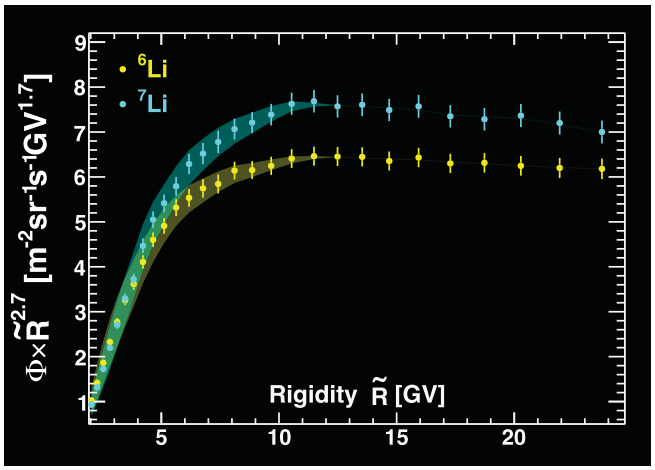

FIG. 3. The AMS time-averaged $\Phi^{^6\mathrm{Li}}$ (yellow) and $\Phi^{^7\mathrm{Li}}$ (cyan) multiplied by $\tilde{R}^{2.7}$ with total errors as functions of rigidity, together with the flux time variations, yellow and cyan bands, respectively.

To study the rigidity dependence of $\Phi^{^7\mathrm{Li}}/\Phi^{^6\mathrm{Li}}$, it has been fitted over the entire rigidity range with

$$\Phi^{^7\mathrm{Li}}/\Phi^{^6\mathrm{Li}} = \begin{cases} C(R/R_0)^{\delta}, & R \le R_0, \\ C, & R > R_0. \end{cases} \quad (4)$$

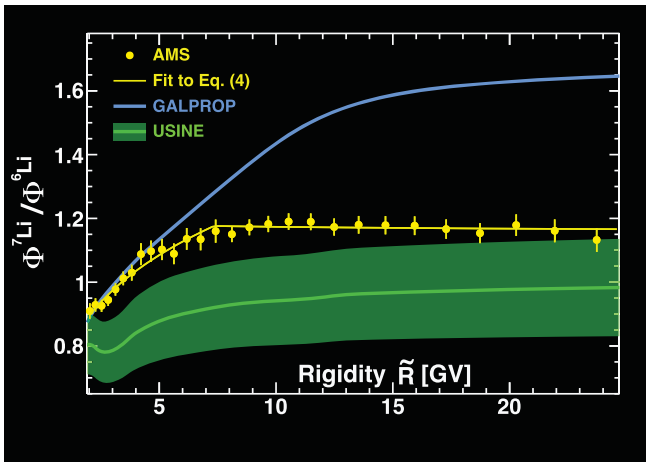

FIG. 4. The AMS time-averaged $\Phi^{^7\mathrm{Li}}/\Phi^{^6\mathrm{Li}}$ with total errors as a function of rigidity, together with the predictions of the recent propagation models GALPROP including a primary $^7\mathrm{Li}$ component in the flux [10] (blue curve) and USINE assuming secondary origin of $^6\mathrm{Li}$ and $^7\mathrm{Li}$ [11] (green curve with shaded area). The green shaded area shows the uncertainty in the ratio due to uncertainties related to the $^6\mathrm{Li}$ and $^7\mathrm{Li}$ production cross sections from heavier nuclei. In both model predictions, the time-averaged solar modulation [45] corresponding to the AMS data taking period is used. Variation of model predictions due to solar modulation uncertainty is negligible. The solid yellow curve shows the fit result with Eq. (4). As seen, the $\Phi^{^6\mathrm{Li}}$ and $\Phi^{^7\mathrm{Li}}$ have an identical rigidity dependence above ~7 GV.

The fit yields $C = 1.17 \pm 0.02$, $\delta = 0.21 \pm 0.01$, and $R_0 = 7.2 \pm 0.4$ GV with a χ^2/d.o.f. of 23.9/25, see Fig. 4. This shows that $\Phi^{^6\mathrm{Li}}$ and $\Phi^{^7\mathrm{Li}}$ have an identical rigidity dependence above ∼7 GV, see further discussion and Fig. S14 in Supplemental Material [23].

This observation shows that both ^{6}Li and ^{7}Li are produced by collisions of heavier cosmic-ray nuclei with the interstellar medium and excludes the existence of a sizable primary component in the ^{7}Li flux. As an example, using the AMS O flux [46] as an estimator of the primary ^{7}Li flux rigidity dependence, and the AMS measured ^{6}Li flux rigidity dependence for the secondary ^{7}Li flux rigidity dependence, we find the primary component in the ^{7}Li flux is $< 3\%$ at 90% confidence level above 7 GV; see further discussion and Fig. S15 in Supplemental Material [23].

In conclusion, precision measurements of the cosmic-ray ^{6}Li and ^{7}Li fluxes have been presented in the rigidity range from 1.9 to 25 GV. We observed that over the entire rigidity range the ^{6}Li and ^{7}Li fluxes exhibit nearly identical time variations and, above ∼4 GV, the time variations of ^{6}Li, ^{7}Li, He, Be, B, C, N, and O fluxes are identical. Above ∼7 GV, we found an identical rigidity dependence of the ^{6}Li and ^{7}Li fluxes. This shows that both ^{6}Li and ^{7}Li are produced by collisions of heavier cosmic-ray nuclei with the interstellar medium and excludes the existence of a sizable primary component in the ^{7}Li flux.

Acknowledgments—We are grateful for important physics discussions with Igor Moskalenko and Subir Sarkar. We thank former NASA Administrator Daniel S. Goldin for his dedication to the legacy of the ISS as a scientific laboratory and his decision for NASA to fly AMS as a DOE payload. We also acknowledge the continuous support of the NASA leadership, particularly Ken Bowersox and of the JSC and MSFC flight control teams that have allowed AMS to operate optimally on the ISS for over 13 years. We are grateful for the support of Regina Rameika and Glen Crawford of the DOE including resources from the National Energy Research Scientific Computing Center under Contract No. DE-AC02-05CH11231. We gratefully acknowledge the strong support from CERN including Fabiola Gianotti and the CERN IT department. We also acknowledge the continuous support from MIT and its School of Science, Nergis Mavalvala, and the Laboratory for Nuclear Science, Boleslaw Wyslouch. Research supported by: Chinese Academy of Sciences, Institute of High Energy Physics, National Natural Science Foundation (NSFC), and Ministry of Science and Technology, National Key R&D Program Grants No. 2022YFA1604802 and No. 2022YFA1604803, NSFC Grant No. 12275158, and Grant No. 12305119, the China Scholarship Council, Shandong University, and the Shandong Institute of Advanced Technology, China; Research Council of Finland, Project No. 321882, and Finnish Academy of Sciences and Letters, Grant No. 301123, Finland; CNRS/IN2P3 and CNES, France; DLR under Grant No. 50OO1803 and computing support on the JARA Partition of the RWTH Aachen supercomputer, Germany; INFN and ASI under ASI-INFN Agreement No. 2021-43-HH.0, and ASI-University of Perugia Agreement No. 2019-2-HH.0, and the Italian Ministry of University and Research (MUR) through the program "Dipartimenti di Eccellenza 2023-2027" (Grant SUPER-C), Italy; the Consejo Nacional de Humanidades, Ciencias y Tecnologías (CONAHCYT) under Grant No. CF-2019/2042 and UNAM, Mexico; NWO under Grant No. 680-1-004, Netherlands; FCT under Grant No. 2024.00992.CERN, Portugal; CIEMAT, IAC, CDTI, MCIN-AEI, and ERDF under Grants No. PID2022-137810NB-C21/C22, No. PCI2023-145945-2, No. PCI2023-145961-2, No. CEX2019-000920-S, and No. JDC2022-049705-I, Spain; the Fondation Dr. Manfred Steuer and the Fondation Ernst et Lucie Schmidheiny, Switzerland; Academia Sinica, the National Science and Technology Council (NSTC), formerly the Ministry of Science and Technology (MOST), under Grants No. 111-2123-M-001-004 and No. 111-2112-M-006-029, High Education Sprout Project by the Ministry of Education at National Cheng Kung University, Taiwan; the Turkish Energy, Nuclear and Mineral Research Agency (TENMAK) under Grant No. 2020TAEK(CERN)A5.H1.F5-26, Türkiye; and NSF Grant No. 2013228 and ANSWERS proposals No. 2149809, No. 2149810, and No. 2149811, LWS NASA Grant/Cooperative Agreement No. 80NSSC20K1819, and FINESST NASA Grant No. 80NSSC21K1392 U.S. Research was also supported by INFN and ASI under ASI-INFN Agreement No. 2019-19-HH.0 and its amendments, Italy.

Data availability—The data that support the findings of this article are openly available [23], embargo periods may apply.

[1] K. Lodders, Solar Elemental Abundances, Planetary Science (2020); J. A. Johnson, B. D. Fields, and T. A. Thompson, The origin of the elements: A century of progress, Phil. Trans. R. Soc. A **378**: 20190301 (2020).

[2] I. A. Grenier, J. H. Black, and A. W. Strong, The nine lives of cosmic rays in galaxies, Annu. Rev. Astron. Astrophys. **53**, 199 (2015); P. Blasi, The origin of galactic cosmic rays, Astron. Astrophys. Rev. **21**, 70 (2013); A. W. Strong, I. V. Moskalenko, and V. S. Ptuskin, Cosmic-ray propagation and interactions in the galaxy, Annu. Rev. Nucl. Part. Sci. **57**, 285 (2007); A. Castellina and F. Donato, Diffusion coefficient and acceleration spectrum from direct measurements of charged cosmic ray nuclei, Astropart. Phys. **24**, 146 (2005).

[3] M. Spite and F. Spite, Lithium abundance at the formation of the Galaxy, Nature (London) **297**, 483–485 (1982); R. H. Cyburt, B. D. Fields, K. A. Olive, and T. H. Yeh, Big Bang

nucleosynthesis: Present status, Rev. Mod. Phys. **88**, 015004 (2016).

[4] E. M. Burbidge, G. R. Burbidge, W. A. Fowler, and F. Hoyle, Synthesis of the elements in stars, Rev. Mod. Phys. 1957) 547 ,**29**); E. Vangioni-Flam, M. Casse, B. D. Fields, and K. A. Olive, LiBeB production by nuclei and neutrinos, Astrophys. J. **468**, 199 (1996); N. Prantzos, Production and evolution of Li, Be, and B isotopes in the galaxy, Astron. Astrophys. **542**, A67 (2012).

[5] A. Tajitsu, K. Sadakane, H. Naito, A. Arai, and W. Aoki, Explosive lithium production in the classical nova V339 Del (Nova Delphini 2013), Nature (London) **518**, 381 (2015); L. Izzo *et al.*, Early optical spectra of nova V1369 can show the presence of lithium, Astrophys. J. **808**, L14 (2015); N. Kawanaka and S. Yanagita, Cosmic-ray lithium production at the nova eruptions followed by a type Ia supernova, Phys. Rev. Lett. **120**, 041103 (2018).

[6] M. Lemoine, E. Vangioni-Flam, and M. Cassé, Galactic cosmic rays and the evolution of light elements, Astrophys. J. **499**, 735 (1998); V. Tatischeff and S. Gabici, Particle acceleration by supernova shocks and spallogenic nucleosynthesis of light elements, Annu. Rev. Nucl. Part. Sci. **68**, 377 (2018); R. Diehl, A. J. Korn, B. Leibundgut, M. Lugaro, and A. Wallner, Cosmic nucleosynthesis: A multi-messenger challenge, Prog. Part. Nucl. Phys. **127**, 103983 (2022).

[7] R. H. Cyburt, B. D. Fields, and K. A. Olive, An update on the Big Bang nucleosynthesis prediction for ^{7}Li: the problem worsens, J. Cosmol. Astropart. Phys. 11 (2008) 012; J. E. Norris, D. Yong, A. Frebel, and S. G. Ryan, A critique of the Spite Plateau and the astration of primordial lithium, Mon. Not. R. Astron. Soc. **522**, 1358 (2023); B. D. Fields, P. Molaro, and S. Sarkar, Big Bang nucleosynthesis, in S. Navas, *et al.* (Particle Data Group), Review of particle physics, Phys. Rev. D **110**, 030001 (2024).

[8] M. Aguilar *et al.*, Observation of new properties of secondary cosmic rays lithium, beryllium, and boron by the Alpha Magnetic Spectrometer on the International Space Station, Phys. Rev. Lett. **120**, 021101 (2018).

[9] M. Aguilar *et al.*, The Alpha Magnetic Spectrometer (AMS) on the International Space Station: Part II—Results from the first seven years, Phys. Rep. **894**, 1 (2021).

[10] M. J. Boschini *et al.*, Deciphering the local interstellar spectra of secondary nuclei with the galprop/helmod framework and a hint for primary lithium in cosmic rays, Astrophys. J. **889**, 167 (2020). In particular, see Fig. 10.

[11] D. Maurin, E. Ferronato Bueno, Y. Génolini, L. Derome, and M. Vecchi, The importance of Fe fragmentation for LiBeB analyses: Is a Li primary source needed to explain AMS-02 data?, Astron. Astrophys. **668**, A7 (2022). We are grateful to D. Maurin for providing the cosmic ray propagation model USINE prediction for the ^{7}Li/^{6}Li flux ratio as a function of rigidity.

[12] P. De La Torre Luque, M. N. Mazziotta, F. Loparco, F. Gargano, and D. Serini, Implications of current nuclear cross sections on secondary cosmic rays with the upcoming DRAGON2 code, J. Cosmol. Astropart. Phys. 03 (2021) 099.

[13] M. Korsmeier and A. Cuoco, Implications of lithium to oxygen AMS-02 spectra on our understanding of cosmic-ray diffusion, Phys. Rev. D **103**, 103016 (2021).

[14] M. Garcia-Munoz, G. M. Mason, and J. A. Simpson, The isotopic composition of galactic cosmic ray lithium, beryllium and boron, Astrophys. J. **201**, L145 (1975).

[15] W. R. Webber, J. A. Lezniak, J. C. Kish, and G. A. Simpson, A measurement of the abundance of cosmic ray ^{10}Be and its implications for the cosmic ray age, Astrophys. Lett. **18**, 125 (1977); W. R. Webber and J. Kish, Further studies of the isotopic composition of cosmic ray Li, Be and B nuclei—implications for the cosmic ray age, *International Cosmic Ray Conference 1979* (1979), Vol. 1, p. 389, https://adsabs.harvard.edu/full/1979ICRC....1..389W.

[16] A. Lukasiak, F. B. McDonald, and W. R. Webber, Voyager measurements of the isotopic composition of Li, Be and B nuclei, *International Cosmic Ray Conference 1997* (1997), Vol. 3, p. 389, https://adsabs.harvard.edu/full/1997ICRC...3..389L; W. R. Webber, A. Lukasiak, and F. B. McDonald, *Voyager* measurements of the charge and isotopic composition of cosmic ray Li, Be, and B nuclei and implications for their production in the galaxy, Astrophys. J. **568**, 210 (2002).

[17] S. P. Ahlen *et al.*, Measurement of the isotopic composition of cosmic-ray helium, lithium, beryllium, and boron up to 1700 MeV per atomic mass unit, Astrophys. J. **534**, 757 (2000).

[18] T. Hams *et al.*, Measurement of the abundance of radioactive ^{10}Be and other light isotopes in cosmic radiation up to 2 GeV nucleon^{-1} with the Balloon-borne Instrument ISOMAX, Astrophys. J. **611**, 892 (2004).

[19] M. Aguilar *et al.*, The Alpha Magnetic Spectrometer (AMS) on the International Space Station: Part I—results from the test flight on the space shuttle, Phys. Rep. **366**, 331 (2002); M. Aguilar *et al.*, Relative composition and energy spectra of light nuclei in cosmic rays: Results from AMS-01, Astrophys. J. **724**, 329 (2010); Isotopic composition of light nuclei in cosmic rays: Results from AMS-01, Astrophys. J. **736**, 105 (2011).

[20] G. A. de Nolfo *et al.*, Observations of the Li, Be, and B isotopes and constraints on cosmic-ray propagation, Adv. Space Res. **38**, 1558 (2006).

[21] W. Menn *et al.*, Lithium and beryllium isotopes with the PAMELA experiment, Astrophys. J. **862**, 141 (2018); F. Nozzoli and C. Cernetti, Beryllium radioactive isotopes as a probe to measure the residence time of cosmic rays in the galaxy and halo thickness: A "data-driven" approach, Universe **7**, 183 (2021); E. A. Bogomolov *et al.*, Lithium and beryllium isotopes in the PAMELA experiment, Bull. Russ. Acad. Sci.: Phys. **87**, 863 (2023).

[22] A. Kounine, The Alpha Magnetic Spectrometer on the International Space Station, Int. J. Mod. Phys. E **21**, 1230005 (2012); S. Ting, The Alpha Magnetic Spectrometer on the International Space Station, Nucl. Phys. B, Proc. Suppl. **243–244**, 12 (2013); B. Bertucci, The AMS-02 detector operation in space, *Proc. Sci.*, EPS-HEP2011 (2011) 67; M. Incagli, Astroparticle physics with AMS02, AIP Conf. Proc. **1223**, 43 (2010); R. Battiston, The antimatter spectrometer (AMS-02): A particle physics detector in space, Nucl. Instrum. Methods Phys. Res., Sect. A **588**, 227 (2008).

[23] See Supplemental Material at http://link.aps.org/supplemental/10.1103/PhysRevLett.134.201001 for the details of the AMS detector description, event selection,

background estimation, fitting procedure, rigidity and velocity resolution functions, further studies on the $\Phi^{7\mathrm{Li}}/\Phi^{6\mathrm{Li}}$ rigidity dependence, estimation of primary ^{7}Li flux fraction, and figures, along with the tabulated time dependence and time average of the ^{6}Li and ^{7}Li fluxes, and the $^7\mathrm{Li}/^6\mathrm{Li}$ flux ratio.

[24] K. Lübelsmeyer *et al.*, Upgrade of the Alpha Magnetic Spectrometer (AMS-02) for long term operation on the International Space Station (ISS), Nucl. Instrum. Methods Phys. Res., Sect. A **654**, 639 (2011).

[25] B. Alpat *et al.*, The internal alignment and position resolution of the AMS-02 silicon tracker determined with cosmic-ray muons, Nucl. Instrum. Methods Phys. Res., Sect. A **613**, 207 (2010).

[26] G. Ambrosi, V. Choutko, C. Delgado, A. Oliva, Q. Yan, and Y. Li, The spatial resolution of the silicon tracker of the Alpha Magnetic Spectrometer, Nucl. Instrum. Methods Phys. Res., Sect. A **869**, 29 (2017).

[27] Y. Jia, Q. Yan, V. Choutko, H. Liu, and A. Oliva, Nuclei charge measurement by the Alpha Magnetic Spectrometer silicon tracker, Nucl. Instrum. Methods Phys. Res., Sect. A **972**, 164169 (2020).

[28] Q. Yan and V. Choutko, Alignment of the Alpha Magnetic Spectrometer (AMS) in space, Eur. Phys. J. C **83**, 245 (2023).

[29] V. Bindi *et al.*, Calibration and performance of the AMS-02 time of flight detector in space, Nucl. Instrum. Methods Phys. Res., Sect. A **743**, 22 (2014).

[30] M. Aguilar *et al.*, In-beam aerogel light yield characterization for the AMS RICH detector, Nucl. Instrum. Methods Phys. Res., Sect. A **614**, 237 (2010); F. Giovacchini, The RICH detector of the AMS-02 experiment aboard the International Space Station, Nucl. Instrum. Methods Phys. Res., Sect. A **1055**, 168434 (2023).

[31] M. Aguilar *et al.*, Precision measurement of the helium flux in primary cosmic rays of rigidities 1.9 GV to 3 TV with the Alpha Magnetic Spectrometer on the International Space Station, Phys. Rev. Lett. **115**, 211101 (2015).

[32] J. Allison *et al.*, Recent developments in GEANT4, Nucl. Instrum. Methods Phys. Res., Sect. A **835**, 186 (2016); J. Allison *et al.*, Geant4 developments and applications, IEEE Trans. Nucl. Sci. **53**, 270 (2006); S. Agostinelli *et al.*, GEANT4 a simulation toolkit, Nucl. Instrum. Methods Phys. Res., Sect. A **506**, 250 (2003).

[33] C. C. Finlay *et al.*, International geomagnetic reference field: The eleventh generation, Geophys. J. Int. **183**, 1216 (2010); E. Thébault *et al.*, International geomagnetic reference field: the 12th generation, Earth Planets Space **67**, 79 (2015); P. Alken *et al.*, International geomagnetic reference field: The thirteenth generation, Earth Planets Space **73**, 49 (2021).

[34] M. Aguilar *et al.*, Precision measurement of the proton flux in primary cosmic rays from rigidity 1 GV to 1.8 TV with the Alpha Magnetic Spectrometer on the International Space Station, Phys. Rev. Lett. **114**, 171103 (2015).

[35] M. Aguilar *et al.*, Properties of cosmic helium isotopes measured by the Alpha Magnetic Spectrometer, Phys. Rev. Lett. **123**, 181102 (2019).

[36] Q. Yan, V. Choutko, A. Oliva, and M. Paniccia, Measurements of nuclear interaction cross sections with the Alpha Magnetic Spectrometer on the International Space Station, Nucl. Phys. **A996**, 121712 (2020).

[37] Note that the data can also be downloaded in different formats from the AMS website https://ams02.space/sites/default/files/publication/202404/table-s1-s42.csv and https://ams02.space/sites/default/files/publication/202404/table-s43.csv, the ASI cosmic-ray database at https://tools.ssdc.asi.it/CosmicRays, and the LPSC cosmic-ray database at https://lpsc.in2p3.fr/crdb/.

[38] D. Maurin, M. Ahlers, H. Dembinski, A. Haungs, P.-S. Mangeard, F. Melot, Ph. Mertsch, D. Wochele, and J. Wochele, A cosmic-ray database update: CRDB v4.1, Eur. Phys. J. C **83**, 971 (2023).

[39] M. Aguilar *et al.*, Properties of daily helium fluxes, Phys. Rev. Lett. **128**, 231102 (2022). The He flux data up to October 2023 including the 12.5-yr time-averaged flux can be downloaded from https://ams02.space/sites/default/files/publication/202404/helium-table-4BR.csv, https://ams02.space/sites/default/files/publication/202404/helium-table-average.csv.

[40] M. Aguilar *et al.*, Solar modulation of cosmic nuclei over a solar cycle: Results from the Alpha Magnetic Spectrometer, Phys. Rev. Lett. **134**, 051001 (2025). In particular, see Fig. 3.

[41] M. Aguilar *et al.*, Properties of cosmic deuterons measured by the Alpha Magnetic Spectrometer, Phys. Rev. Lett. **132**, 261001 (2024).

[42] G. D. Lafferty and T. R. Wyatt, Where to stick your data points: The treatment of measurements within wide bins, Nucl. Instrum. Methods Phys. Res., Sect. A **355**, 541 (1995). We have used Eq. (6) with $\tilde{R} \equiv x_{lw}$.

[43] Y. Génolini, D. Maurin, I. V. Moskalenko, and M. Unger, Current status and desired precision of the isotopic production cross sections relevant to astrophysics of cosmic rays. II. Fluorine to silicon and updated results for Li, Be, and B, Phys. Rev. C **109**, 064914 (2024); I. V. Moskalenko (private communication).

[44] M. J. Boschini *et al.*, Inference of the local interstellar spectra of cosmic-ray nuclei $Z \leq 28$ with the GalProp–HelMod framework, Astrophys. J. **250**, 27 (2020).

[45] M. S. Potgieter, Solar modulation of cosmic rays, Living Rev. Solar Phys. **10**, 3 (2013); I. G. Usoskin, A. Gil, G. A. Kovaltsov, A. L. Mishev, and V. V. Mikhailov, Heliospheric modulation of cosmic rays during the neutron monitor era: Calibration using PAMELA data for 2006–2010, J. Geophys. Res. Space Phys. **122**, 3875 (2017). Recent data are taken from the University of Oulu website https://cosmicrays.oulu.fi/phi/phi.html.

[46] M. Aguilar *et al.*, Observation of the identical rigidity dependence of, He, C, and O cosmic rays at high rigidities by the Alpha Magnetic Spectrometer on the International Space Station, Phys. Rev. Lett. **119**, 251101 (2017). The 12.5-yr time-averaged O flux used in this work can be downloaded from https://ams02.space/sites/default/files/publication/202404/oxygen-table-average.csv.

Correction: A missing funding statement has been inserted in the Acknowledgments section.